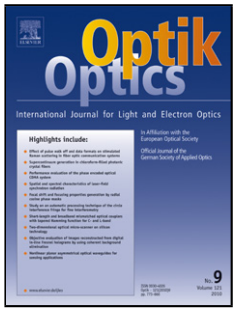

Title: Two layers Corrugated semiconductor Solar cell

Authors: Hala J El-Khozondar, Ahmed A. Alshembari, Mohammed M. Shabat, Alexander W. Koch

PII: S0030-4026(18)32072-2
DOI: https://doi.org/10.1016/j.ijleo.2018.12.138
Reference: IJLEO 62155

To appear in:

Received date: 8 December 2018
Accepted date: 26 December 2018

Please cite this article as: El-Khozondar HJ, Alshembari AA, Shabat MM, Koch AW, Two layers Corrugated semiconductor Solar cell, *Optik* (2018), https://doi.org/10.1016/j.ijleo.2018.12.138

Two layers Corrugated semiconductor Solar cell

Hala J El-Khozondar[a,*] , Ahmed A. Alshembari[b]
Mohammed M. Shabat[c], Alexander W. Koch[d]

[a]*Department of Electrical Engineering, Islamic University of Gaza, Gaza Strip, Palestine; Email: hkhozondar@iugaza.edu.ps*
[b]*Department of Industrial Mathematics, Technische Universität Kaiserslautern, Germany, Email:a.shembari@gmail.com*
[c]*Department of Physics, Faculty of Science, Islamic University of Gaza, Gaza Strip, Palestine*
[d] *Department of Electrical and Computer Engineering, Institute for Measurement Systems and Sensor Technology, Theresienstrasse 90, N5, Munich, Germany*

*Corresponding author
Email:hkhozondar@iugaza.edu.ps (H.J.El-Khozondar)

Abstract

A new two-layer-waveguide solar cell is introduced. It consists of silicon monoxide (SiO) layer on top of Fe-InGaAsP film surrounded by Air cladding and transparent conducting oxides (TCO) substrate. Both TE and TM reflection and transmission powers have been extracted from the Hybrid Transfer Matrix Method. The average transmitted, reflected and absorbed power as function of the operating wavelength have been computed and plotted numerically for several physical parameters as the layers' thicknesses, type of materials and the incidence angles. The simulations have been carried out by using the MAPLE software. The results show that changing the type of TCO layer does not affect the performance of the solar cell. Thus, for low moisture environment, AZO is better choice than ITO. However, we noticed that the thickness of each layer and the incidence angle have considerable effect on the performance of the solar cell. This work has shown excellent results for high transmission of the incident waves frequency bands. Hence, the studied structure would be promising to be utilized in the field of solar cells.

Keywords: transparent conducting oxides; solar cell; Transmission and reflection powers; waveguides.

I. Introduction

Harnessing solar energy to obtain electrical energy is a priority in the world to overcome environmental problem results from using fossil sources of energy. This required high efficiency solar cells.

Different techniques has been used to obtain high efficiency solar cells including using antireflection coating (ARC) double layer [1-3] or single layer [4-5]. In addition, different type of materials have been used to construct the stack of layers of the solar cell in purpose of studying the effect of each material on the solar cell performance. For example researchers used metamaterials to enhance the performance of solar cell [4-5], nanocomposite materials [6], single crystalline materials [7-8] , polycrystalline materials [9], organic materials and inorganic materials [10-11] and quantum dots [12].

Metallic structures paid a lot of attention for their applications in spectroscopy [13] and nanophotonics [14]. Transparent conducting oxides (TCOs) has been introduced as replacement of plasmonic materials [15].

The focus of the paper is to explore the possibilities of combining different materials for the layers of a solar cell and calculation of the optimum thickness of these layers with the objective of less reflection and high absorption using. In particular, we interested to see the efficiency enhancement using transparent conducting oxides (TCO). The choice of a transparent conductive oxide (TCO) as the contact of a PV cell is critical for long term performance of the cell. PV with TCO has low contact resistance, low bulk resistance and has a low drying temperature of less than $200\ ^{0}$ C [16]. TCO are transparent in the visible range due to the fact that they have a large bandgap [17-18].

In Section 2, the TCOs such as AluminumZinkoxide (AZnO) and indium tin oxide (ITO) are discussed. Section 3 will describe the proposed model and its mathematical mechanism. Finally, in Section 4, conclusions are provided.

II. The TCOs such as ITO and ZnO

Aluminum Zinc Oxide (AZO) is also another common TCO. It has low cost and relatively good optical transmission performance in the solar spectrum. However, if even the slightest amount of moisture penetrates the cell, the AZO coating reacts with the water and ceases to operate as a TCO, rendering the cell useless.

Indium tin oxide (ITO) has high electrical conductivity and optical transparency. Also, it can be easily deposited as a thin film. It is a ternary composition of indium, tin and oxygen in varying proportions. Depending on the oxygen content, it can either be described as a ceramic or alloy. It is transparent and colorless in thin layers. Thin films of indium tin oxide are most commonly deposited on surfaces by physical vapor deposition. When deposited as a thin film on glass or clear plastic it functions as a transparent electrical conductor.

The main concern about another TCO, indium tin oxide (ITO) is the cost. ITO can be priced at several times that of AZO. However, ITO does consistently defeat AZO in almost every performance category including chemical resistance to moisture. ITO is not affected by moisture and it can survive in a PV for 25-30 years on a rooftop [19]

The dielectric function of the materials may be approximated in the wavelength range of 350–2000 nm by the Drude–Lorentz model as in equation (1).

$$\varepsilon_{tco}(\omega) = \varepsilon_b - \frac{\omega_p^2}{\omega\left(\omega + i\,\gamma_p\right)} + \frac{f_1\omega_1^2}{\left(\omega_1^2 + \omega^2 + i\,\omega\gamma_p\right)} \tag{1}$$

where the values of the parameters are listed in the table below [20].

Table 1. Drude–Lorentz parameters of two alternative plasmonic materials retrieved from ellipsometry measurements.

Item	**AZO**	**ITO**
ε_b	3.5402	3.528
$\omega_p[eV]$	1.7473	1.78
$\gamma_p[eV]$	0.04486	0.155
f_1	0.5095	0.3884
$\omega_1[eV]$	4.2942	4.210
$\gamma_1[eV]$	0.1017	0.0919

III. Proposed Model and Mathematical Representation

The proposed solar cell consist of four layers stratified in ẑ direction as can be seen in Figure 1. The four layers are: air cover with refractive index, $n_0 \approx 1$, silicon monoxide (*SiO*) with $n_1 \approx 1.7369$ [21] and thickness l_1, Iron- indium Gallium arsenide phosphide (*Fe-InGaAsP*) has $n_2 \approx 3.3723\text{-}0.0024*i$ [22, 23] and thickness l_2, the *TCO* has ε_{tco}. All the media are considered to be nonmagnetic media such that $\mu = 1$.

For each layer (s =0, 1, 2, 3) of thickness l_s, its upper and lower bounding interfaces are denoted by $Z_s^>$ and $Z_s^<$ respectively. The homogeneous medium of each layer is characterized by permittivity ε_S and permeability μ_S.

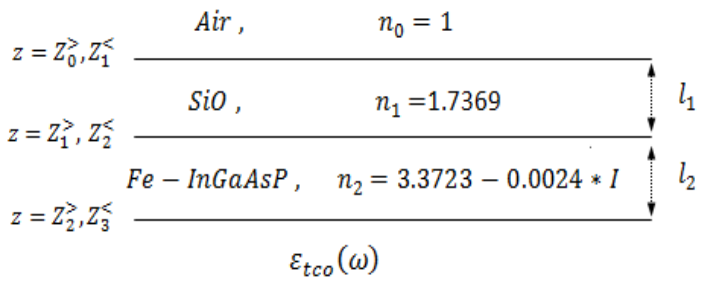

Figure 1: The proposed four layer waveguide structure.

According to [24] the reflection and transmission behavior of a set of stacked layer/s on the top of a substrate with different materials and/or different compositions can be described using the 2x2 matrices (**S** matrix). This is possible because the equations governing the propagation of electric field are linear and tangential component of the electric field is continuous [25].

To find the transfer matrix for TE mode equation (2), we choose $E_x\left(Z_1^{<>}\right)=0$ and $H_y\left(Z_1^{<>}\right)=0$. The matrix is in

$$\begin{bmatrix} E_y(z_1^{\langle}) \\ H_x(z_1^{\langle}) \end{bmatrix} = \begin{bmatrix} m_{22} & m_{23} \\ m_{32} & m_{33} \end{bmatrix} \begin{bmatrix} E_y(z_1^{\rangle}) \\ H_x(z_1^{\rangle}) \end{bmatrix} \tag{2}$$

The reflectance and transmittance for TE mode are obtained through the reflection and transmission coefficients. The reflection coefficient (r_{TE}) is given by:

$$r_{TE} = \frac{m_{22}\beta_0 + m_{23}\beta_0\beta_s - m_{32} - m_{33}\beta_s}{m_{22}\beta_0 + m_{23}\beta_0\beta_s + m_{32} + m_{33}\beta_s} \tag{3}$$

where,

$$\beta_i = \frac{k_{iz}}{\mu_i} = \frac{ki}{\mu_i}\cos(\theta_i) \quad i=0,\ 1,\ S \tag{4}$$

The reflectance equation (R_{TE}) is

$$R_{TE} = |r|^2 = r \cdot r^* \tag{5}$$

The transmission coefficient (t_{TE}) can be written as,

$$t_{TE} = \frac{2\beta_0}{m_{22}\beta_0 + m_{23}\beta_0\beta_s + m_{32} + m_{33}\beta_s} \tag{6}$$

The transmittance equation (T_{TE}) is given by,

$$T_{TE} = \frac{\beta_S}{\beta_0}|t|^2 = \frac{\beta_S}{\beta_0}(t \cdot t^*) \tag{7}$$

Following similar approach to find the transfer matrix for TM mode and taking $E_y\left(Z_1^{\diamond}\right) = 0$ and $H_x\left(Z_1^{\diamond}\right) = 0$, we get:

$$\begin{bmatrix} E_x(z_1^{\langle}) \\ H_y(z_1^{\langle}) \end{bmatrix} = \begin{bmatrix} m_{11} & m_{14} \\ m_{41} & m_{44} \end{bmatrix} \begin{bmatrix} E_x(z_1^{\rangle}) \\ H_y(z_1^{\rangle}) \end{bmatrix} \tag{8}$$

The reflection coefficient (r_{TM}) can be expressed as,

$$r_{TM} = \frac{m_{41}\gamma_0\gamma_s + m_{44}\gamma_0 - m_{11}\gamma_s - m_{14}}{m_{41}\gamma_0\gamma_s + m_{44}\gamma_0 + m_{11}\gamma_s + m_{14}} \tag{9}$$

where $\gamma_i = \frac{k_{iz}}{\varepsilon_i} = \frac{ki}{\varepsilon_i}\cos(\theta_i)$, i=0, 1, s.

The reflectance power (R_{TM}) is given by

$$R_{TM} = |r|^2 = r \cdot r^* \tag{10}$$

The transmission coefficient (t_{TM}) can be represented by the following formula,

$$t_{TM} = \frac{2\gamma_0}{m_{41}\gamma_0\gamma_s + m_{44}\gamma_0 + m_{11}\gamma_s + m_{14}} \tag{11}$$

The transmittance power (T_{TM}) is

$$T_{TM} = \frac{\gamma_S}{\gamma_0}|t|^2 = \frac{\gamma_S}{\gamma_0}(t \cdot t^*) \tag{12}$$

The sun light has both polarization. We consider the sun light as hybrid mode that consists of both polarization. Thus, to calculate the reflectance and transmittance power of the solar radiation, we take the average of TE and TM modes.

$$R_{avg} = \frac{R_{TE} + R_{TM}}{2} \tag{13}$$

$$T_{avg} = \frac{T_{TE} + T_{TM}}{2} \tag{14}$$

IV. Numerical simulation and discussions

Minimum reflectance and maximum Absorption in the visible light region are basic requirements and key issues in design solar cells. Therefore, we solved equations (13, 14) to obtain average reflectance and average transmittance. We repeated the calculations two times one using AZO and second time using ITO.

First we done the following calculation while using AZO:

For normal incidence, the average reflectance (R_{avg}) versus the operating light wavelength for different values of the *SiO* thickness (l_1) has been simulated and plotted in Figure 2. It can be seen that as λ increases R_{avg} begins to decrease until it reaches its minimum value around λ= 570 nm for l_1 = 110 nm. This minimum varies as l_1 changes. It actually occurs at smaller values of λ as l_1 decreases. The minimum value of R_{avg} occurs around λ = 480 nm and 530 nm for l_1 = 90 nm and 100 nm respectively. Furthermore, the minima locations have been observed in the visible light spectrum. The value l_1 = 110 nm is considered the best thickness because the minimum reflectance appears close to the mid of the visible light range, λ = 570 nm. In addition, this figure demonstrates that the minimum reflectance is shifting towards higher wavelengths as the thickness l_1 increases.

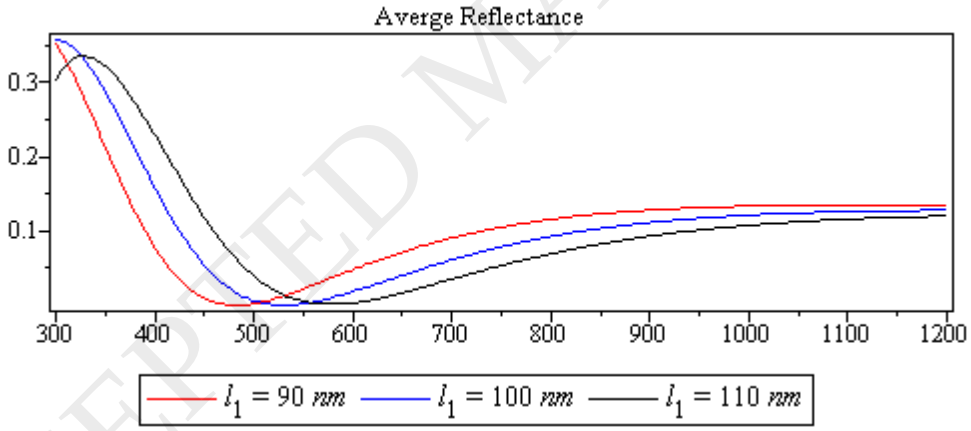

Figure 2: The average reflection power (R_{avg}) as function of λ at different values of l_1.

Figure 3 displays the average transmittance (T_{avg}) versus the operating wavelength λ. We notice that transmittance has opposite values of the reflectance. The average absorption (A_{avg}) was calculated from the conventional relation $A_{avg}(\lambda) = 1 - R_{avg}(\lambda) - T_{avg}(\lambda)$. Then, A_{avg} was plotted as a function of the wavelength in Figure 4. It is observed from this figure that the maximum absorption in visible light range is decreasing with increasing the *SiO* thickness (l_1).

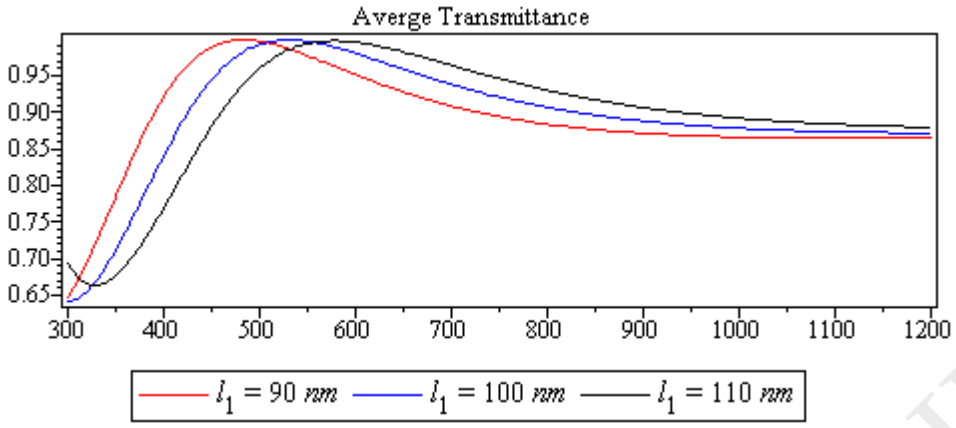

Figure 3: The average transmission power (T_{avg}) as function of λ at different values of l_1

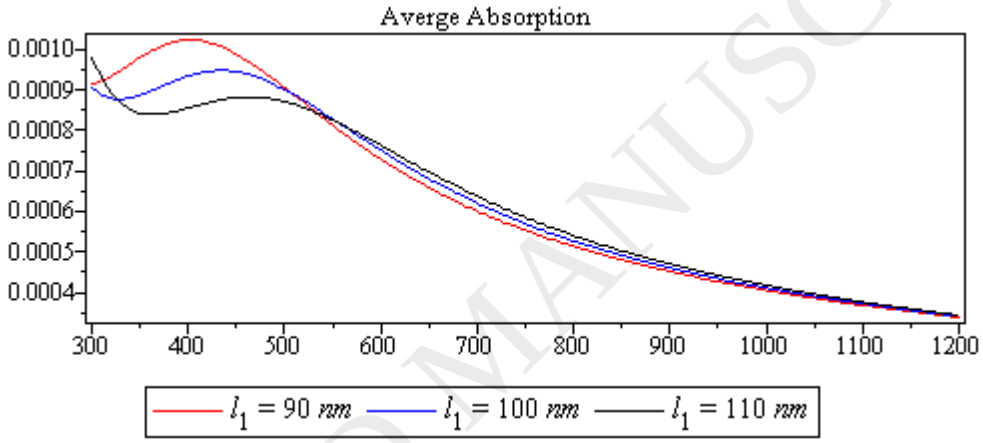

Figure 4: The average absorption power (A_{avg}) as function of λ at different values of l_1

Figure 5 displays the relation between R_{avg} and λ at various thicknesses of *InP* (l_2). The minimum R_{avg} occurs at different λ values as l_2 varies. In the calculation we assumed l_2=*5nm* , *10nm* and *20nm*. We realized the minimum occurs at l_2=10 nm around 540nm.

The relationship between the T_{avg} and λ is shown in Figure 6. Figure 6 shows that the maximum T_{avg} decreases as l_2 increases. Figure 7 demonstrates the A_{avg} versus wavelength for different thicknesses of l_2. It is noticed that the absorption rises as the thickness of *InP* increases.

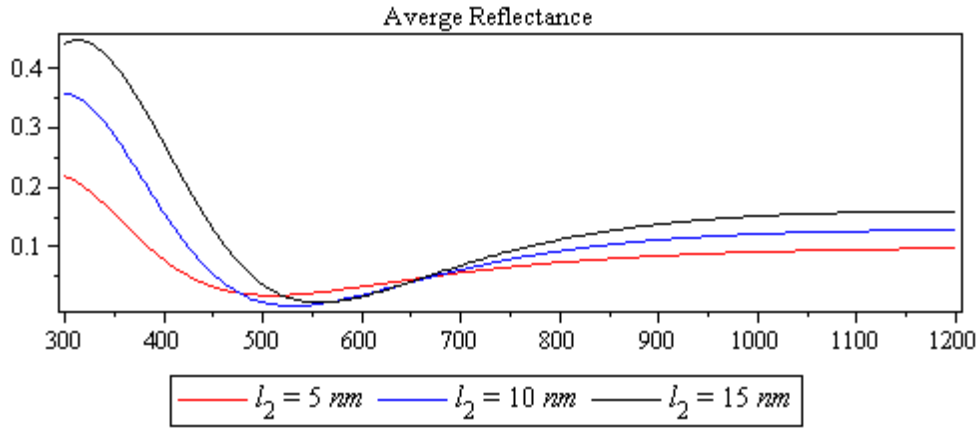

Figure 5: The average reflection power (R) as function of wavelength (λ) at different values of l_2

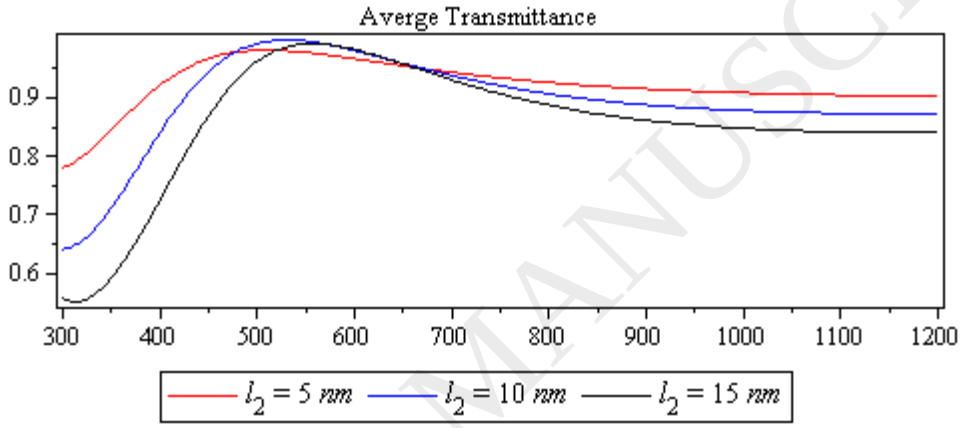

Figure 6: The average transmission power (T_{avg}) as function of wavelength (λ) at different values of l_2

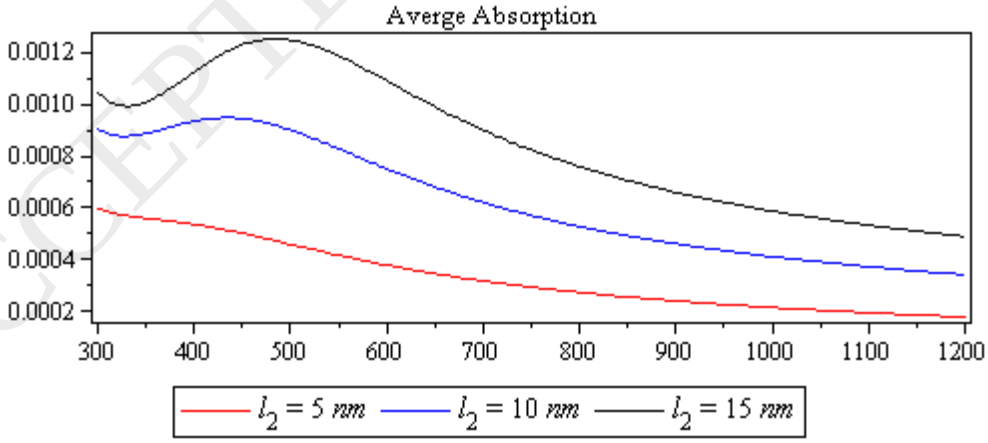

Figure 7: The average absorption power (A_{avg}) as function of wavelength (λ) at different values of l_2

For glance incidence, R_{avg} as function of λ is shown in figure 8. As θ_0 changes form normal incidence (0^0) to 30^0 and 60^0 , the minimum value changes its value and position. From figure 8, we can see that minimum occurs at λ=500nm when θ_0= 30^0 . The average transmittance power and absorption power are shown in figure 9 and 10 respectively.

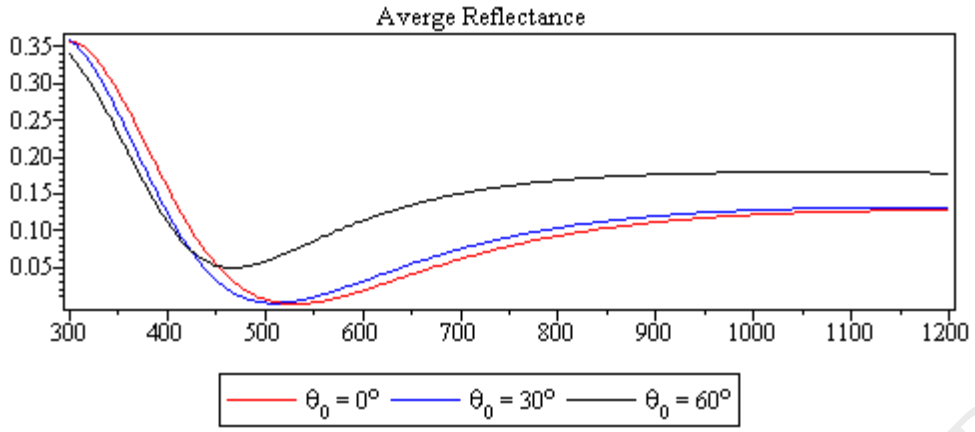

Figure 8: The average refection power (R_{avg}) as function of wavelength (λ) at different values of θ_0

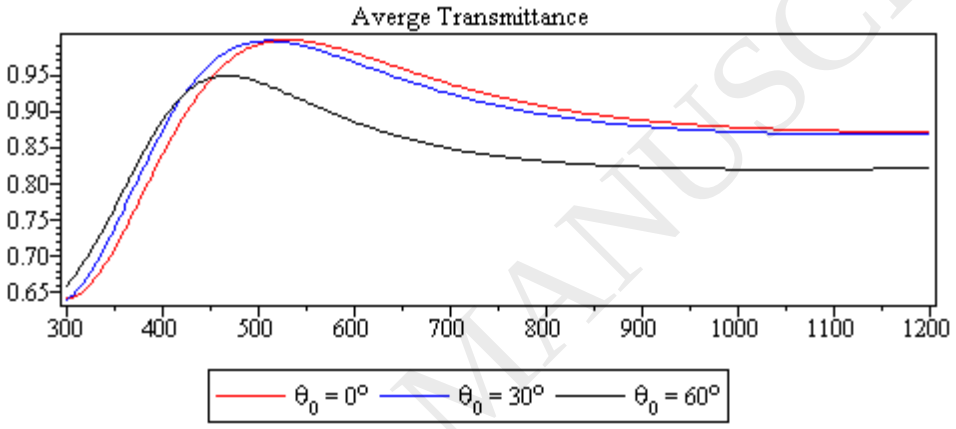

Figure 9: The average transmittance power (T_{avg}) as function of wavelength (λ) at different values of θ_0

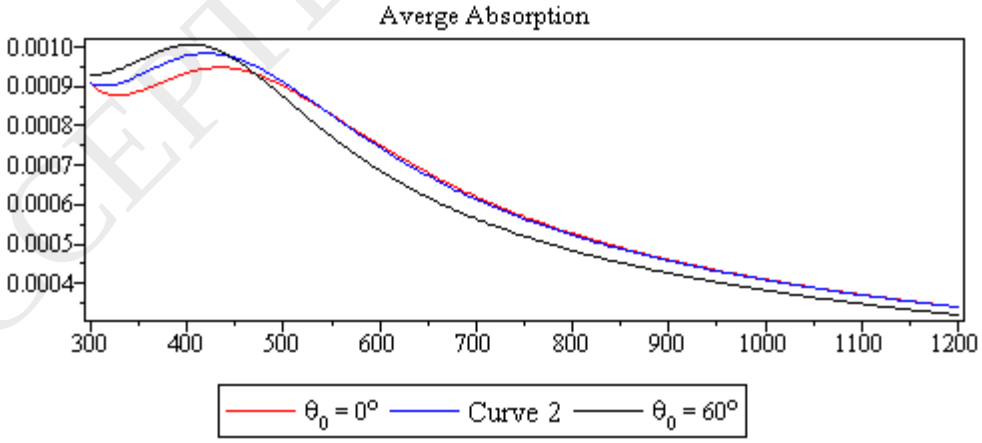

Figure 10: The average absorption power (A_{avg}) as function of wavelength (λ) at different values of θ_0

Second, we redone the above calculations using ITO:
Figures 11, 12 and 13 display respectively R_{avg}, T_{avg} and A_{avg} as function of λ at different values of l_1. We noticed that the changes are small compared when we used AZO. The values of R_{avg}, T_{avg} and A_{avg} versus λ at different values of l_2 are exhibited on figures 14, 15 and 16 respectively.

The results looks very similar to what we have obtained for using AZO. Finally, for the plots at glancing incidence which have been displayed on figures 17, 18 and 19 gave also similar results as the one we got for AZO.

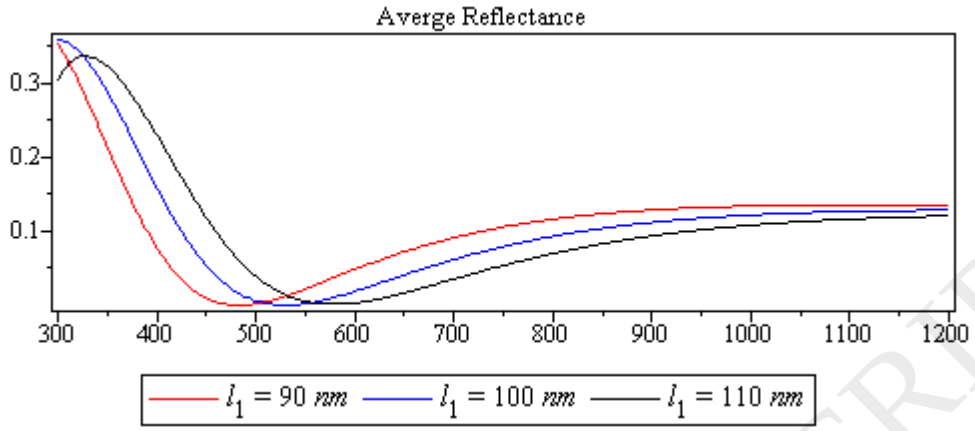

Figure 11: The average reflection power (R_{avg}) as function of λ at different values of l_1.

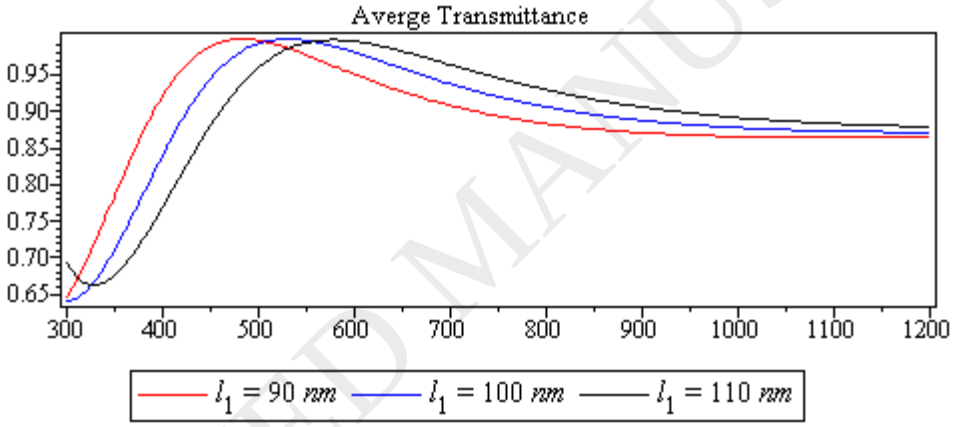

Figure 12: The average transmittance power (T_{avg}) as function of λ at different values of l_1.

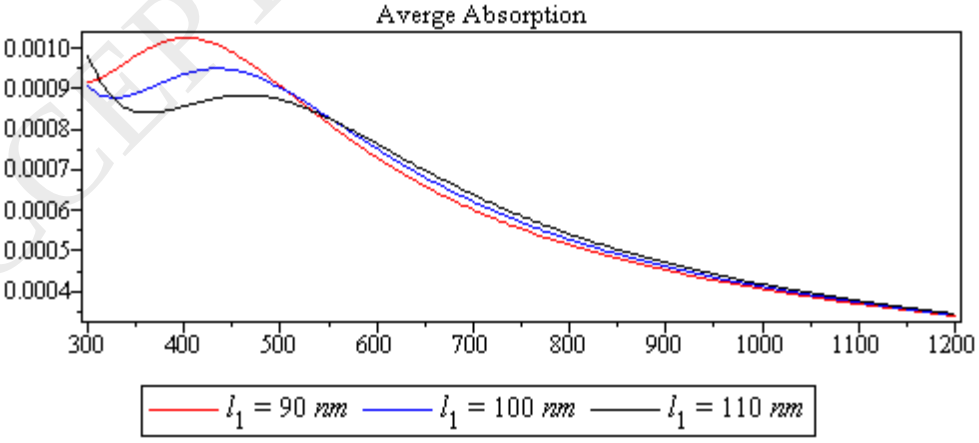

Figure 13: The average absorption power (A_{avg}) as function of λ at different values of l_1.

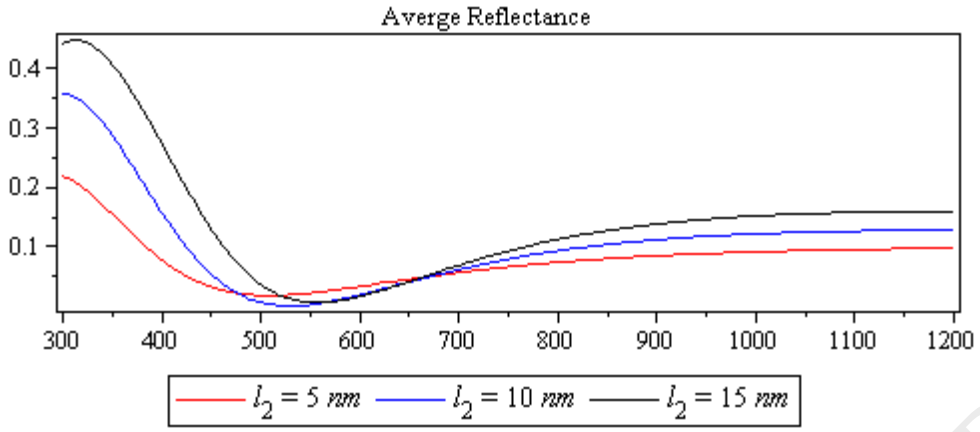

Figure 14: The average reflection power (R_{avg}) as function of wavelength (λ) at different values of l_2

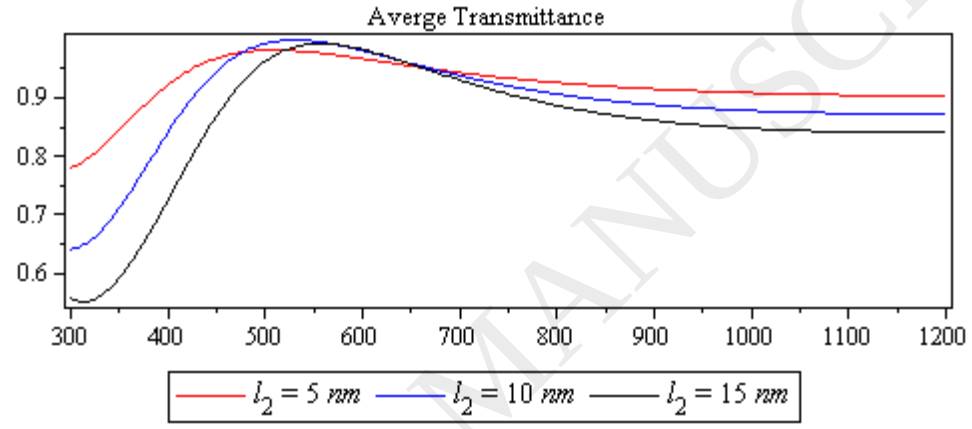

Figure 15: The average transmission power (T_{avg}) as function of wavelength (λ) at different values of l_2

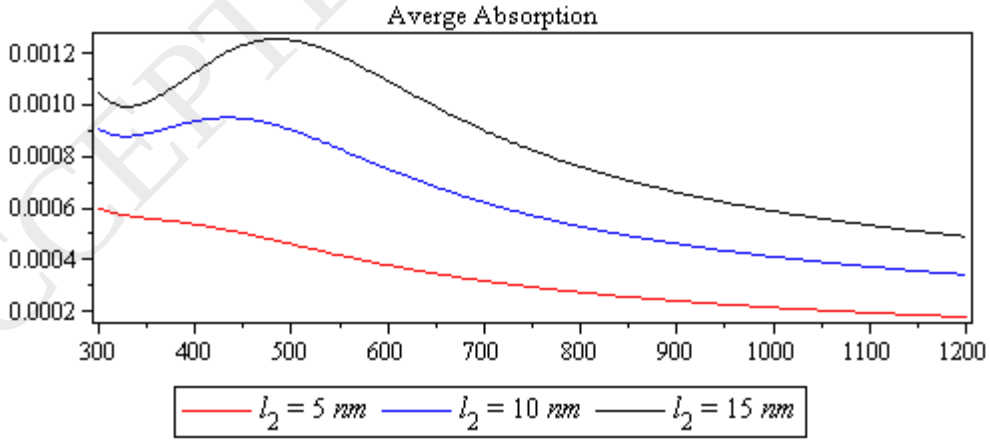

Figure 16: The average absorption power (A_{avg}) as function of wavelength (λ) at different values of l_2

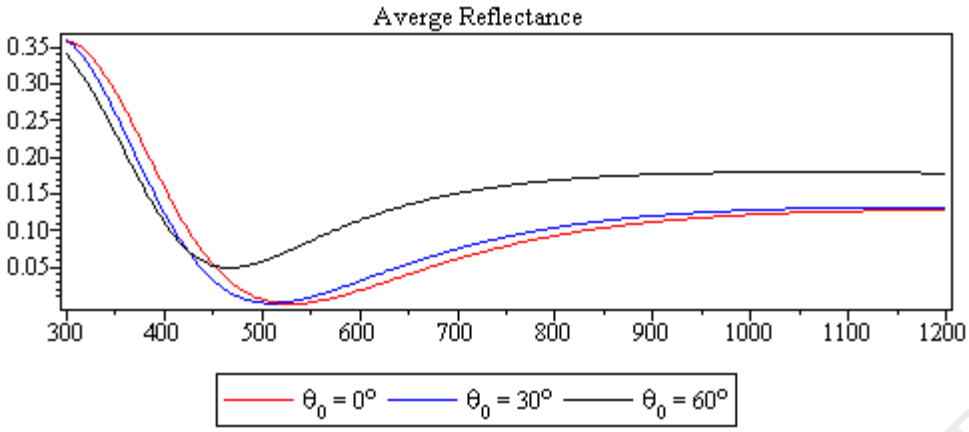

Figure 17: The average refection power (R_{avg}) as function of wavelength (λ) at different values of θ_0

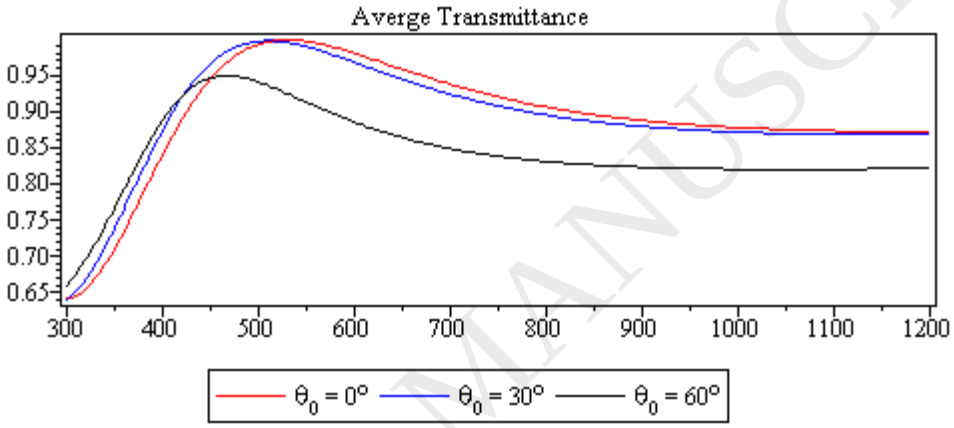

Figure 18: The average transmittance power (T_{avg}) as function of wavelength (λ) at different values of θ_0

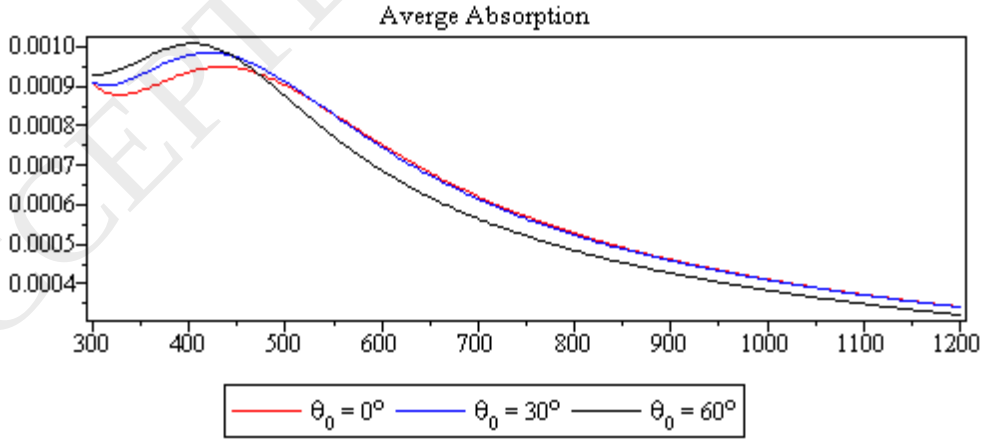

Figure 19: The average absorption power (A_{avg}) as function of wavelength (λ) at different values of θ_0

V. Conclusion

In this work, a new solar cell waveguide is introduced. Air cladding and transparent conducting oxides (TCO) substrate surrounding silicon monoxide (SiO) and Fe-InGaAsP two layers. The Transfer Matrix Method (TMM) is used to calculate the transmission, reflection and absorption powers. The mentioned powers are calculated and plotted as function of operating wavelength using Maple software. Different parameters are considered in the calculations like the type of TCO material, the layers' thicknesses and the incident angle.

Results present that the type of TCO makes no difference on the results while layers' thicknesses and incident angle affects the results. Therefore, one can choose cheap AZO compared to ITO for several application without worrying about the performance of the cell. However, in cases where moisture is an issue then ITO is the better choice. In addition, we can optimize the solar cell structure by tuning the layers' thicknesses and the incident angle value. This work present promising results for solar cell fabrications.

References

1. H. Taguchi, T. Soga, T. Jimbo, Fabrication of GaAs/Si tandem solar cell by epitaxial lift-off technique. Japanese Journal of Applied Physics Part 2-letters 42 (2003) L1419-1421.
2. C. E .Valdivia, E. Desfonds, D. Masson, S. Fafard, A. Carlson, J. Cook, T. J. Hall, K. Hinzer, *Optimization of antireflection coating design for multi-junction solar cells and concentrator systems, Request PDF*. Available from: https://www.researchgate.net/publication/268273732_Optimization_of_antireflection_coating_design_for_multi-junction_solar_cells_and_concentrator_systems [accessed Sep 25 2018].
3. Optimization of antireflection coating design for multi-junction solar cells and concentrator systems, Proceedings of the society of Photo-Optical Instrumentation Engineers (2008) 7099.
4. M. Beye, M. Faye, A. Ndiaye, F. Ndiaye, A.S. Maiga, Optimization of SiNx Single and Double Layer ARC for Silicon Thin Film Solar Cells on Glass, Research Journal of Applied Sciences, Engineering and Technology 6 (2013) 412-416.
5. D. M. El-Amassi, H. J. El-Khozondar, M. M. Shabat, Efficiency Enhancement of Solar Cell Using Metamaterials, International Journal of Nano Studies & Technology (IJNST) 4(2015) 84-87.
6. H.J. El-Khozondar, D.M. El-Amassi, M.M. Shabat, Modification of PV behavior using dissipative MTM, META'15:The 6th International Conference on Metamaterials, Photonic Crystals and Plasmonics, Ed. Said Zouhdi, Vinod M. Menon, New York, USA (2015) 303-304.

7. H.J. El-Khozondar, R. J. El-Khozondar, M.M. Shabat, D. M. Schaadt, Solar cell with multilayer structure based on nanoparticles composite, *OPTIK* 166 (2018) 127–131.
8. H. Sai, T. Matsui, T. Koida, K. Matsubara, M. Kondo, S. Sugiyama, H. Katayama, Y. Takeuchi, and I. Yoshida, Triplejunction thin-film silicon solar cell on periodically textured substrate with a stabilized efficiency of 13.6%, Appl. Phys. Lett. 106 (2015) 213902.
9. M. Yamaguchi, H. Yamada, Y. Katsumata, K. Lee, K. Araki, & N. Kojima, Efficiency potential and recent activities of high-efficiency solar cells, Journal of Materials Research 32 (2017) 3445-3457.
10. T. J. Coutts, et al., J. S. Ward, D. L. Young, K. A. Emery, T. A. Gessert, R. Noufi, Critical issues in the design of polycrystalline, thin film tandem solar cells. *Progress in photovoltaics: Research and Applications*, 11.6 (2003): 359-375.
11. X. Xu, K. Fukuda, A. Karki, S. Park, H. Kimura, H. Jinno, N. Watanabe, S. Yamamoto, S. Shimomura, D. Kitazawa, T. Yokota, S. Umezu, T. Nguyen, and T. Somey, Thermally stable, highly efficient, ultraflexible organic photovoltaics, PNAS Latest Articles (2018) 1 of 6, www.pnas.org/cgi/doi/10.1073/pnas.1801187115.
12. N. J. Jeon, J. H. Noh, Y. C. Kim, W. S. Yang, S. Ryu, S. Seok, Solvent engineering for high-performance inorganic–organic hybrid perovskite solar cells, Nature Materials 13 (2014) 897–903.
13. E. M. Sanehira, A. R. Marshall, J. A. Christians, S. P. Harvey, P. N. Ciesielski, L. M. Wheeler, P. Schulz, L. Y. Lin, M. C. Beard, J. M. Luther, Enhanced mobility CsPbI3 quantum dot arrays for record-efficiency, high-voltage photovoltaic cells, Science Advances 3 (2017) 1-8.
14. C. L. Haynes, A. D. McFarland, R. P. Duyne, Surface-enhanced: raman spectroscopy, Anal. Chem. 77 (2005) 338A–346A.
15. D. K. Gramotnev, S. I. Bozhevolnyi, Plasmonics beyond the diffraction limit, Nature Photonics 4 (2010) 83–91.
16. T. Gric, Spoof plasmons in corrugated transparent conducting oxides, Journal of Electromagnetic Waves and Applications 30 (2016) 721–727.
17. http://www.indium.com/blog/low-temperature-metallization-paste.php.
18. T. Minami, Transparent conducting oxide semiconductors for transparent electrodes, Semicond. Sci. Technol. 20 (2005) S35–S44.
19. G. J. Exarhos, X. D. Zhou, Discovery-based design of transparent conducting oxide films, Thin Solid Films 515 (2007) 7025–7052.
20. http://www.indium.com/blog/tco-choices-for-cigs-manufacturing.php
21. G. V. Naik, V. M. Shalaev, A. Boltasseva, Alternative plasmonic materials: beyond gold and silver. Adv. Materials 25 (2013) 3264–3294.
22. H. J. El-Khozondar, M. M. Shabat, A. N. Alshembari, Characteristics of Si-Solar cell (PV) Waveguide Structure Using Transfer Matrix Method, 2017 International Conference on Promising Electronic Technologies (ICPET), Deir El-Balah, Palestine, (2017).
23. T. M. Hartnett, S. D. Bernstein, E. A. Maguire & R. W. Tustison, Optical properties of ALON (aluminum oxynitride). Infrared Physics & Technology 39 (1998) 203-211.
24. A. Fekecs, M. Chicoine, B. Ilahi, A. J. SpringThorpe, F. Schiettekatte, D. Morris, P. G. Charette, R. Arès, Critical process temperatures for resistive InGaAsP/InP heterostructures heavily implanted by Fe or Ga ions, Nuclear Instruments and Methods

in Physics Research Section B: Beam Interactions with Materials and Atoms 359 (2015) 99-106
25. R. M. Bashar, *Ellipsometry and Polarized Light.* Amsterdam: North Holland, (1977).
26. T. Zhan, X. Shi, Y. Dai, X. Liu and J. Zi, Journal Phys., Transfer matrix method for optics in graphene layers, Condens. Matter 25 (2013) 215301(1-10).